Nanomed Res J 10(1):81-94, Winter 2025

RESEARCH ARTICLE

Enhancing the Anti-Breast Cancer Activity of Eugenol Using a Magnesium Oxide Nanoparticle-Based Delivery System

Fahad Al-Mohanna[1], Shahrzad Shahbazi[2], Somayeh Reiisi[1*]

[1] Department of Genetics, Faculty of Basic Sciences, Shahrekord University, Shahrekord, Iran

[2] Division of Genetics, Department of Cell and Molecular Biology and Microbiology, Faculty of Biological Science and Technology, University of Isfahan, Isfahan, Iran

ARTICLE INFO

Article History:
Received 06 Dec 2024
Accepted 13 Feb 2025
Published 01 Mar 2025

Keywords:
Eugenol
Magnesium oxide nanoparticles
Drug delivery
Breast cancer
Apoptosis
Oxidative stress

ABSTRACT

Objective(s): Eugenol, a natural phenolic compound, exhibits diverse biological properties, including antimicrobial, antioxidant, anti-inflammatory, and anticancer activities. Magnesium oxide nanoparticles (MgONPs) have emerged as efficient nanocarriers for drug delivery due to their biocompatibility and stability. This study investigated the anticancer potential of free eugenol and eugenol-loaded MgONPs (MgONPs@Eugenol) against MDA-MB-231 human breast cancer cells.

Methods: MgONPs were synthesized and loaded with eugenol, followed by characterization using Fourier-transform infrared spectroscopy (FTIR) and X-ray diffraction (XRD), DLS, ZETA and Electron microscopy. The cytotoxic effects of free eugenol, bare MgONPs, and MgONPs@Eugenol were evaluated using the MTT assay in MDA-MB-231 cells and normal HUVEC cells. A scratch assay assessed cell migration, and gene expression analysis was conducted using qPCR to evaluate the expression of apoptosis-related (CASP3, CASP8, CASP9, Bcl-2) and oxidative stress-related genes (SOD2, CAT, GPx).

Results: The nanoparticles exhibited a crystalline structure with an average size of 215.2 nm, a polydispersity index (PDI) of 0.089, and a zeta potential of –15.48 mV. The results demonstrated that MgONPs@Eugenol significantly enhanced cytotoxicity, reduced cell migration, and promoted apoptosis compared to free eugenol in MDA-MB-231 cells. These effects were associated with the upregulation of pro-apoptotic genes (CASP3, CASP8, CASP9) and gene expression of antioxidant enzymes (SOD2, CAT, GPx), alongside the downregulation of the anti-apoptotic gene Bcl-2.

Conclusions: Eugenol-loaded MgO nanoparticles exhibited superior anticancer activity compared to free eugenol, suggesting their potential as an effective nanocarrier-based therapeutic strategy for the treatment of breast cancer.

How to cite this article
Al-Mohanna F., Shahbazi Sh., Reiisi S. Enhancing the Anti-Breast Cancer Activity of Eugenol Using a Magnesium Oxide Nanoparticle-Based Delivery System. Nanomed Res J, 2024; 10(1): 81-94. DOI: 10.22034/nmrj.2025.01.009

INTRODUCTION

Breast cancer is one of the most frequently diagnosed cancers as well as one of the most leading causes of cancer-related deaths in women worldwide, posing a critical global health concern. Established treatment modalities, such as surgery, chemotherapy, radiotherapy, hormone therapy, and targeted therapy, have undergone substantial progress in recent years and have contributed to better disease management. Despite these advancements, breast cancer still accounts for one of the highest cancer-related mortality rates among women worldwide, particularly in cases involving aggressive subtypes or late-stage diagnosis, highlighting the urgent need for more effective and targeted therapeutic strategies to improve clinical outcomes (1).

Novel therapeutic strategies, such as nanoparticle-based drug delivery systems, have emerged as promising approaches for improving

* Corresponding Author Email: *s.reiisi@yahoo.com*
s.reiisi@sku.ac.ir.

the clinical outcomes of breast cancer treatment (2). These nanotechnology-driven platforms offer several advantages over conventional therapies, including enhanced drug stability, controlled release, and targeted delivery specifically to tumor cells with minimal effects on normal adjacent tissues. Consequently, they reduce systemic toxicity and minimize side effects, such as fatigue, nausea, vomiting, anemia, hair loss, immunosuppression, hepatotoxicity, nephrotoxicity, and cardiotoxicity (3, 4). Furthermore, nanoparticle-based systems improve the bioavailability, biodegradability, and therapeutic efficacy of anticancer agents, helping overcome drug resistance and non-specific distribution, ultimately leading to better treatment responses and improved patient prognosis (5, 6). Nanoparticles also serve as carriers for various therapeutic substances, encompassing chemotherapeutic drugs, nucleic acids, proteins, peptides, and antibiotics (7). Naturally derived compounds have recently been reported to be delivered by various nanoparticles and have demonstrated potential for the treatment of various diseases such as neurodegenerative disorders (8-11), cardiovascular conditions (12, 13), inflammatory diseases (14), neuroplastic diseases (15), and various types of cancers (16-18). Eugenol is a naturally occurring phenolic compound found in clove oils. Eugenol has traditionally been employed in dentistry to relieve tooth pain and in oral care products owing to its soothing effect. In recent years, there has been considerable interest in their potential therapeutic applications comprising antioxidant, antifungal, antibacterial, antiviral, analgesic, antiseptic, antiplatelet, anti-inflammatory, antiallergic, anti-swelling, antioxidant, antimutagenic, and anticancer properties (19-24). Moreover, its biological effects are attributed to its ability to modulate cellular signaling pathways and induce cell death in numerous cancer cell lines (25). Nevertheless, high doses of eugenol can be toxic, making dose regulation essential for clinical and pharmaceutical applications (24). Nanoparticles can be categorized into various types based on their values. For example, based on their composition, they can be classified into organic nanoparticles (such as liposomes, micelles, dendrimers, and polymeric nanoparticles), inorganic nanoparticles (nanoparticles lacking carbon are included as metal-based and metal oxide-based), and carbon-based nanoparticles. Metal oxide-based nanoparticles, such as silicon dioxide nanoparticles (SiO_2 NPs), ferric oxide nanoparticles (Fe_2O_3 NPs), zinc oxide nanoparticles (ZnO NPs), titanium dioxide nanoparticles (TiO_2 NPs), magnesium oxide nanoparticles (MgO NPs), and cerium oxide nanoparticles (CeO NPs) are formed through the combination of positively charged metal ions and negatively charged oxygen ions, resulting in stable ionic structures driven by strong electrostatic forces (26-28). Owing to their distinctive physicochemical characteristics, these materials are utilized in a wide range of fields including healthcare, agriculture, industry, engineering, and the environment (29). Among them, MgO NPs are highly versatile materials, can be synthesized using various methods, and have a unique nanostructure with features such as shape and size tunability, chemical and thermal stability, high surface area, biocompatibility, and biodegradability, which can be applied in various aspects of medicine, including the delivery of several anticancer agents (30, 31). Based on this knowledge, we conducted an in vitro study to evaluate the potential of MgO NPs as a carrier for eugenol, a naturally derived compound, and to assess the anticancer effects of this nanoformulated delivery system.

MATERIALS AND METHODS

Synthesis of Magnesium Oxide Nanoparticles (MgO NPs)

Magnesium oxide nanoparticles (MgO NPs) were synthesized through a controlled precipitation method using magnesium nitrate hexahydrate ($Mg(NO_3)_2{\cdot}6H_2O$) as the precursor. A 0.1 M solution of magnesium nitrate was prepared by dissolving 2.56 g of $Mg(NO_3)_2{\cdot}6H_2O$ in 100 mL of deionized water under constant magnetic stirring. Separately, a 0.4 M sodium hydroxide (NaOH) solution was obtained by dissolving 0.8 g of NaOH in 50 mL of distilled water. The NaOH solution was then added dropwise to the magnesium nitrate solution under continuous stirring to ensure uniform mixing and nucleation. The pH of the reaction medium was carefully adjusted and maintained at 11, as this is a critical parameter that significantly influences nanoparticle formation and morphology. Following pH adjustment, the reaction mixture was stirred for an additional 2 hours and heated to 70 °C to facilitate the formation of a white magnesium hydroxide ($Mg(OH)_2$) precipitate. The suspension was subsequently centrifuged at 10,000 rpm for 10 minutes to collect the precipitate. The resulting

product was washed twice with ethanol and twice with distilled water to remove residual impurities. The purified precipitate was then dried in a vacuum oven at 100 °C for 6 hours. Finally, calcination was carried out at 500 °C for 4 hours in a muffle furnace to convert Mg $(OH)_2$ into crystalline MgO nanoparticles.

Eugenol loading into magnesium oxide nanoparticles

MgO NPs were loaded with eugenol at a ratio of 2:1 and named as MgONPs@Eugenol. An appropriate amount of eugenol was dissolved in 1 mL 96% ethanol by vortex mixing. This eugenol solution was then combined with the MgO NPs suspension and stirred in the dark at 800–1000 RPM for 24 h to facilitate adsorption. Following the incubation period, the mixture was transferred to microcentrifuge tubes and centrifuged at 10,000 RPM for 15 min at 4°C. This process resulted in phase separation, with the supernatant containing unbound (free) eugenol and the precipitate comprising eugenol-loaded magnesium oxide nanoparticles (MgO NPs@Eugenol). The excess liquid was separated from the precipitate and spectrophotometrically analyzed to measure the concentration of free eugenol. The absorbance value was applied to a pre-established eugenol calibration curve to quantify its concentration. The loading efficiency was then calculated using the concentrations of both free and total amounts of eugenol based on the following formula:

$$\text{Eugenol loading efficiency} = \frac{\text{initial concentration of the eugenol} - \text{concentration of free eugenol}}{\text{initial concentration of the eugenol}} \times 100$$

Nanoparticle characterization

A comprehensive set of analytical techniques was employed to characterize the physicochemical properties of both free MgO NPs and eugenol-loaded MgO NPs. Dynamic light scattering (DLS) analysis was performed using a Zetasizer Nano ZS (Malvern Instruments, UK) to determine the hydrodynamic particle size, polydispersity index (PDI), and zeta potential, providing insight into the colloidal stability and particle size distribution in suspension. Fourier transform infrared (FTIR) spectroscopy was carried out using an FT/IR-6300 spectrometer (JASCO, Japan) over the spectral range of 350–4000 cm^{-1} to identify characteristic functional groups and confirm the chemical composition of the nanoparticles. X-ray diffraction (XRD) analysis was conducted using a PHILIPS PW1730 diffractometer (Netherlands) equipped with Cu Kα radiation (λ = 1.54056 Å), operated at 40 kV and 30 mA. The scanning was performed with a step size of 0.05° and a counting time of 1 second per step to determine the crystalline structure and lattice parameters of the MgO NPs. Morphological evaluation was performed using both transmission electron microscopy (TEM) and scanning electron microscopy (SEM), which provided detailed visualization of particle size, shape, and surface morphology. In addition, FTIR and zeta potential analyses were repeated for MgO NPs@Eugenol to assess the loading efficiency. Comparative analysis with bare MgO NPs confirmed successful eugenol loading, as evidenced by spectral shifts and surface charge modification.

Eugenol release from magnesium oxide nanoparticle

An in vitro release study was conducted to evaluate the release profile of eugenol from MgO NPs@Eugenol under simulated physiological (pH 7.2) and tumor microenvironment (pH 4.5) conditions. Phosphate-buffered saline (PBS) solutions were prepared at pH 4.5 and 7.2 to mimic acidic and neutral environments, respectively. A nanoparticle loaded with eugenol (50mg) was prepared, and was added to 0.5mL of each PBS solution at the corresponding pH. The mixtures were transferred into dialysis bags with a molecular weight cut-off (MWCO) of 12 kDa and immersed in 20 mL of PBS buffer at the neutral pH in separate containers. The release system was incubated at 37 °C in a shaker incubator maintained at 100 rpm to simulate physiological conditions. At predetermined time intervals (0.5, 1, 2, 4, 8, 12, 24, 48, and 72 hours), 1 mL of the external PBS medium was withdrawn and immediately replaced with an equal volume of fresh buffer to maintain sink conditions. The concentration of eugenol in the collected samples was quantified using UV–visible spectrophotometry by measuring the absorbance at the characteristic wavelength of eugenol. The cumulative percentage of eugenol released at each time point was calculated using a standard calibration curve and a drug release equation. Based on these measurements, the percentage of eugenol released from the MgO NPs under both acidic and neutral pH conditions was calculated using a standard drug release formula.

Cell culture and cytotoxicity assay

The MDA-MB-231 human breast cancer cell

line, a triple-negative line lacking estrogen receptor (ER) and HER2/neu expression, was obtained from the Iranian Biological Resource Center (IBRC, Tehran, Iran) and utilized as a representative model for metastatic breast cancer. Primary human umbilical vein endothelial cells (HUVECs), isolated from neonatal umbilical cords, were also procured from IBRC and served as a model for normal human cells. Both cell lines were cultured in RPMI-1640 medium supplemented with 10% fetal bovine serum (FBS) and 1% penicillin-streptomycin. Cells were maintained in T25 culture flasks at 37 °C in a humidified atmosphere with 5% CO_2. The cytotoxicity and growth-inhibitory effects of bare MgO NPs, free eugenol, and MgO NPs@Eugenol were evaluated using the MTT colorimetric assay. Cells were seeded in 96-well microplates and allowed to adhere for 24 hours under standard culture conditions. HUVEC cells were then treated with various concentrations of bare MgO NPs (0, 10, 25, 50, 100, 150, 200, and 500 µg/mL), free eugenol (0, 0.5, 1, 2.5, 5, 10, 20, and 50 µg/mL), and MgO NPs@Eugenol (same concentration range as eugenol). After 24, 48, and 72 hours of treatment, 20 µL of MTT reagent was added to each well and incubated for 3 hours to allow for formazan crystal formation. Subsequently, 100 µL of dimethyl sulfoxide (DMSO) was added to dissolve the formazan, and absorbance was measured at 490 nm using a DANA-3200 microplate reader (Iran).

Cell migration assay

A wound-healing (scratch) assay was conducted to assess the migratory capacity of MDA-MB-231 human breast cancer cells. Cells were seeded in 12-well plates and cultured until reaching 90–95% confluency. After 24 hours, a uniform scratch was introduced at the center of each well using a sterile 100 µL pipette tip. Detached cells and debris were removed by washing twice with PBS. Subsequently, cells were treated with the IC30 concentrations (concentrations causing 10% cytotoxicity, as determined by MTT assay) of bare MgO NPs, free eugenol, and MgO NPs@Eugenol. Cell migration and wound closure were monitored by capturing images at 0-, 24-, and 48-hours' post-treatment using an inverted phase-contrast microscope. Quantitative analysis of the wound area was performed using the MRI Wound Healing Tool plugin in ImageJ software (National Institutes of Health, Bethesda, MD, USA), enabling the calculation of the percentage of wound closure over time.

Gene expression analysis

Quantitative real-time PCR (qRT-PCR) was employed to assess the impact of bare MgO NPs, free eugenol, and MgO NPs@Eugenol on the expression of apoptosis-related genes such as caspase-3 (CASP3), CASP8, CASP9, and Bcl-2, in addition to oxidative stress-related genes including SOD2, CAT, and GPx1. MDA-MB-231 breast cancer cells were cultured at a density of 7×10^5 cells per well in 6-well plates. Following a 24-hour incubation, the cells were treated with the IC50 concentration of each compound. Total RNA was extracted using TRIzol reagent (Invitrogen) in accordance with the manufacturer's instructions. The isolated RNA was subsequently reverse-transcribed into cDNA utilizing M-MLV enzyme with oligo (dT) and random hexamer primers (YTA, Iran). qPCR was conducted using SYBR Green Real-Time PCR Master Mix (YTA, Iran) along with the gene-specific primers detailed in Table 1. GAPDH was utilized as an internal reference gene. Amplification was carried out on a Mic-qPCR system, initiating with a denaturation step at 94 °C for 5 minutes, followed by 40 cycles consisting of denaturation at 94 °C for 15 seconds, annealing at the gene-specific temperature for 10 seconds, and extension at 72 °C for 10 seconds. All reactions were performed in triplicate. The relative expression levels of the genes were determined using the $2-\Delta\Delta Ct$ method.

Statistical analysis

Graphical representations and statistical analyses were performed using GraphPad Prism version 8.4 (GraphPad Software, Inc., La Jolla, CA, USA). Statistical significance was assessed using an unpaired Student's *t*-test and one-way analysis of variance (ANOVA) for comparison of two groups and more than two groups, respectively. A *P*-value of less than 0.05 ($P < 0.05$) was considered statistically significant. All *in vitro* experiments were conducted in triplicates.

RESULTS

Magnesium oxide nanoparticles synthesize and characterization

Magnesium oxide nanoparticles (MgO NPs) were synthesized using sodium hydroxide (NaOH) as a precipitating agent, followed by thermal treatment to ensure complete calcination. A comprehensive set of physicochemical characterization analyses was performed to evaluate the properties of the synthesized MgO NPs (Fig. 1).

Table 1. Primer Sequences for Real-Time PCR

Gene name	Sequence (5'->3')	Product size
CASP3	F: TTCTTCACCATGGCTCAGAAGCACAC R: AAGCACTGGAATGACATCTCGGTCTG	202 bp
CASP8	F: ACAAGGGCATCATCTATGGCA R: TCTCGTTTGAGGTGATGATAAATC	218 bp
CASP9	F: GTGGATTGCACGTGGCCTCTT R: TTGGCACCACTCAGGAAGACG	216 bp
BCL2	F: TGGCCTTCTTTGAGTTCGGTG R: GGATCCAGGTGTGCAGGTGC	126 bp
SOD2	F: CTGGACAAACCTCAGCCCTAAC R: ACCTGAGCCTTGGACACCAAC	136 bp
CAT	F: GTGCGGAGATTCAACACTGCCA R: CGGCAATGTTCTCACACAGACG	109 bp
GPx1	F: GTGCTCGGCTTCCCGTGCAAC R: CTCGAAGAGCATGAAGTTGGGC	123 bp
GAPDH	F: ACAACTTTGGTATCGTGGAAGG R: GCCATCACGCCACAGTTTC	101 pb

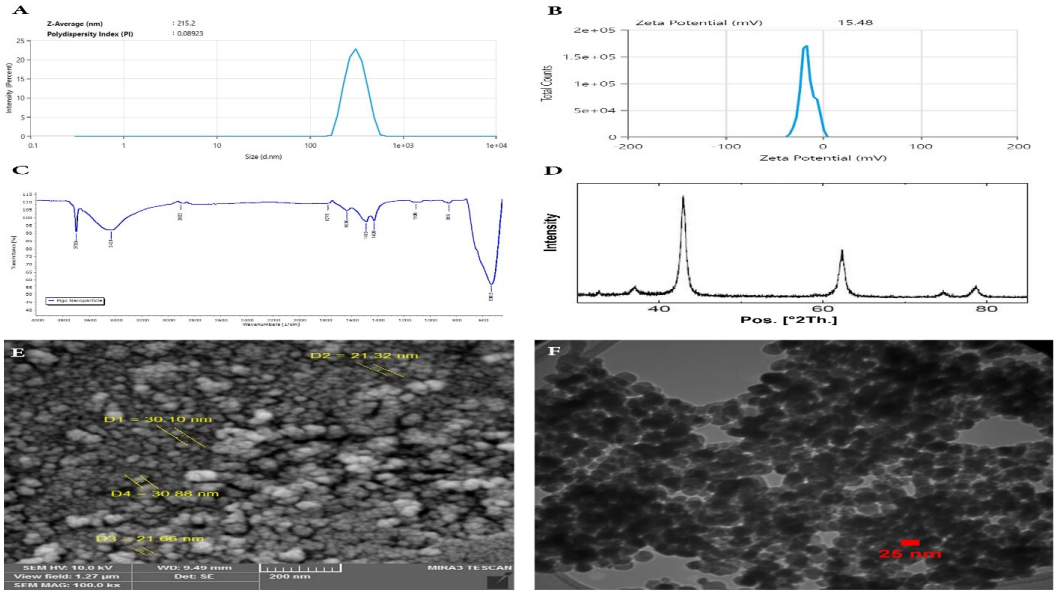

Fig. 1. MgO NPs characterization. A) Size and PDI of MgO NPs determined to be 215.2 nm and 0.089, respectively, through DLS (N=3). B) Zeta potential of MgO NPs obtained using the Zetasizer and found to be -15.48 mV. C) FTIR spectra of MgO NPs. D) XRD pattern of MgO NPs. SEM images of MgO NPs to identify the surface morphology. The scale bars used here is 200 nm. F) TEM image of MgO NPs. The scale bar used here is 25 nm.

Dynamic light scattering (DLS) analysis (Fig. 1A) revealed an average particle size of 215.2 nm and a polydispersity index (PDI) of 0.089, indicating a narrow size distribution and high degree of uniformity. The zeta potential measurement (Fig. 1B) showed a surface charge of −15.48 mV, suggesting adequate colloidal stability and minimal particle agglomeration. Figure 1C presents the Fourier-transform infrared (FTIR) spectrum of the synthesized MgO nanoparticles (NPs), employed to elucidate the chemical bonding and identify the functional groups present on the nanoparticle surface. Distinct absorption bands corresponding to C–C, C–O, and C–N stretching vibrations were observed, indicating the presence of these organic functional groups likely originating from residual precursor materials or surface adsorbates. In the region below 1000 cm^{-1}, characteristic peaks associated with O–H bending and C–O stretching were detected. Notably, a prominent absorption

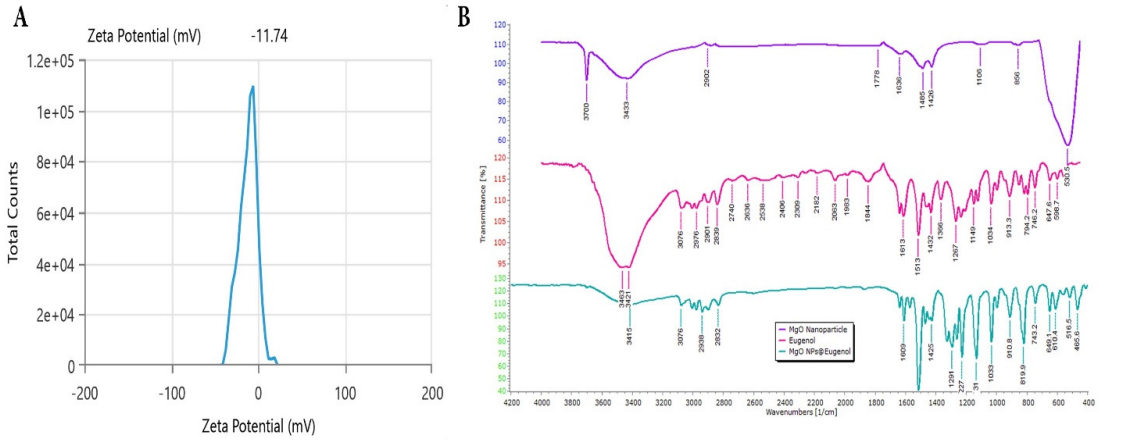

Fig. 2. MgO NPs@Eugenol characterization indicating the successful loading of eugenol into MgO NPs. A) Zeta potential of MgO NPs@Eugenol obtained using the Zeta sizer and found to be -11.74 mV. B) FTIR spectra of MgO NPs, free eugenol, and MgO NPs@ Eugenol.

band within the range of 400–600 cm^{-1} is attributed to Mg–O stretching vibrations, a hallmark of MgO structures. Figure 1D presents the X-ray diffraction (XRD) pattern of the synthesized MgO nanoparticles, revealing a series of well-defined and sharp diffraction peaks indicative of their crystalline nature. Prominent reflections appear at 2θ values of approximately 37°, 43°, 62°, 74°, and 78°, corresponding to the characteristic planes of the face-centered cubic (fcc) phase of MgO. The most intense peak, located near 2θ ≈ 43°, is attributed to the (200) crystallographic plane, while the peaks near 62° and 78° correspond to the (220) and (222) planes, respectively, further confirming the presence of a cubic crystalline structure. The sharpness and intensity of these diffraction peaks reflect a high degree of crystallinity, and the absence of additional peaks confirms the phase purity of the nanoparticles. Figures 3E and 3F depict the morphological features of the MgO NPs as assessed by scanning electron microscopy (SEM) and transmission electron microscopy (TEM), respectively. SEM imaging (Fig. 3E) revealed noticeable agglomeration, a typical behavior for MgO NPs due to their high surface energy and strong van der Waals interactions. The nanoparticles exhibited irregular morphologies, potentially arising from non-uniform crystal growth or partial sintering during calcination. Darker regions in the micrograph reflect areas of increased particle density. In contrast, the high-resolution TEM image (Fig. 3F) provided clearer visualization of individual nanoparticles, which predominantly displayed spherical to slightly irregular shapes with an average diameter of approximately 25 nm—consistent with SEM observations. Despite some degree of agglomeration, the TEM analysis confirmed the presence of well-dispersed particles with clearly defined crystalline structures, corroborating the XRD results.

Eugenol loading into magnesium oxide nanoparticles and validation

To fabricate the eugenol-loaded nanoparticles (MgO NPs@Eugenol), synthesized MgO nanoparticles were combined with eugenol at a 2:1 weight ratio and continuously stirred for 24 hours to facilitate adsorption. The resulting suspension was subjected to centrifugation, followed by repeated washing with ethanol and distilled water to remove any unbound eugenol. The final product was collected and dried for further analysis. The eugenol loading efficiency was calculated to be 95%, indicating highly efficient incorporation of the active compound. To confirm the successful loading and evaluate potential modifications, a series of physicochemical characterizations were performed on the MgO NPs@Eugenol composite. According to Fig.2A, the surface charge of the synthetic MgO NPs was found to be -11.74 mV. Given that eugenol is a neutral (uncharged) molecule, its adsorption onto the MgO NPs surface results in a shift of the zeta potential toward less negative values. Specifically, the zeta potential of the MgO NPs increased from –15.48 mV to –11.74 mV following eugenol loading, indicating a modification of the surface charge and confirming the successful loading of eugenol on the MgO NPs.

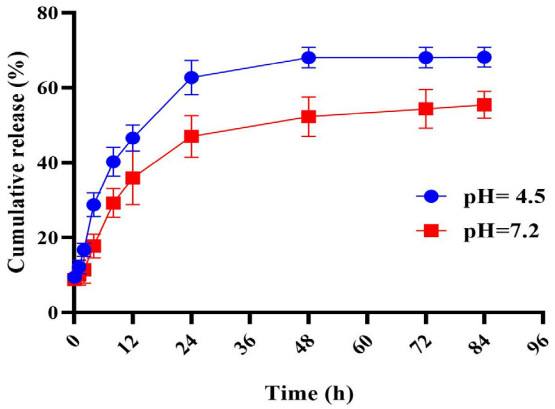

Fig. 3. In vitro drug release assay. The percentage of cumulative release of eugenol from MgO NPs@Eugenol, where blue and red lines indicate pH=4.5 and pH=7.2, respectively, mimic the tumor and physiological conditions, respectively.

Moreover, the functional groups and chemical properties of bare MgO NPs, free eugenol, and MgO NPs @ Eugenol were compared. As shown in Fig.2B, no new peaks were observed in the FTIR spectrum of MgO NPs @ Eugenol compared to the spectra of bare MgO NPs and free eugenol. Furthermore, none of the characteristic peaks disappeared, and all absorption bands remained within their expected wavenumber ranges. The presence of overlapping peaks suggests the absence of any significant chemical interactions between eugenol and the MgO NPs, indicating that eugenol maintained its original chemical structure upon loading, and the interaction with the MgO NPs was likely physical rather than chemical in nature.

Eugenol release from magnesium oxide nanoparticles

The release behavior of eugenol from MgO NPs@ Eugenol was evaluated under two physiologically relevant pH conditions—pH 4.5 (acidic) and pH 7.2 (neutral)—to mimic the tumor microenvironment and normal physiological conditions, respectively. The release experiments were conducted using a dialysis bag diffusion technique, and the concentration of eugenol released at various time intervals was quantitatively determined via UV-Vis spectroscopy. As illustrated in Figure 3, eugenol release was markedly enhanced at acidic pH compared to neutral conditions, highlighting the pH-sensitive release characteristics of the nanocomposite. This pH-responsive behavior is particularly advantageous for targeted drug delivery in acidic tumor environments. Moreover, the release profile demonstrated a sustained release pattern extending over 72 hours, indicating a gradual and controlled diffusion of eugenol from the nanoparticle matrix. The release plateaued after 84 hours, beyond which no significant additional release was detected, suggesting the near-complete exhaustion of the loaded drug.

Cell proliferative assay

The cytotoxic effects of bare MgO NPs, free eugenol, and MgO NPs@Eugenol were systematically assessed using the MTT assay in both normal cells (HUEVCs) and MDA-MB-231 breast cancer cells. Treatments were administered at concentrations ranging from 0 to 500 µg/mL for bare MgO NPs, and from 0 to 50 µg/mL for both free eugenol and MgO NPs@Eugenol. Cell viability was measured at 24, 48, and 72 h post-treatment to evaluate both time- and concentration-dependent effects. As shown in Figure 4, all tested formulations exhibited low cytotoxicity toward HUEVCs, with only a marginal decrease in cell viability observed across all time points, underscoring the biocompatibility of the treatments with normal cells. In contrast, Figure 5 demonstrates a pronounced cytotoxic effect on MDA-MB-231 breast cancer cells, with cell viability significantly reduced in a dose- and time-dependent manner. Among the tested groups, MgO NPs@Eugenol exhibited the most potent antiproliferative activity, with IC_{50} values consistently below 10 µg/mL at all-time intervals. The calculated IC_{50} values for each formulation in both normal and cancer cell lines are summarized in Table 2.

Cell migration assay

The anti-migratory effects of bare MgO

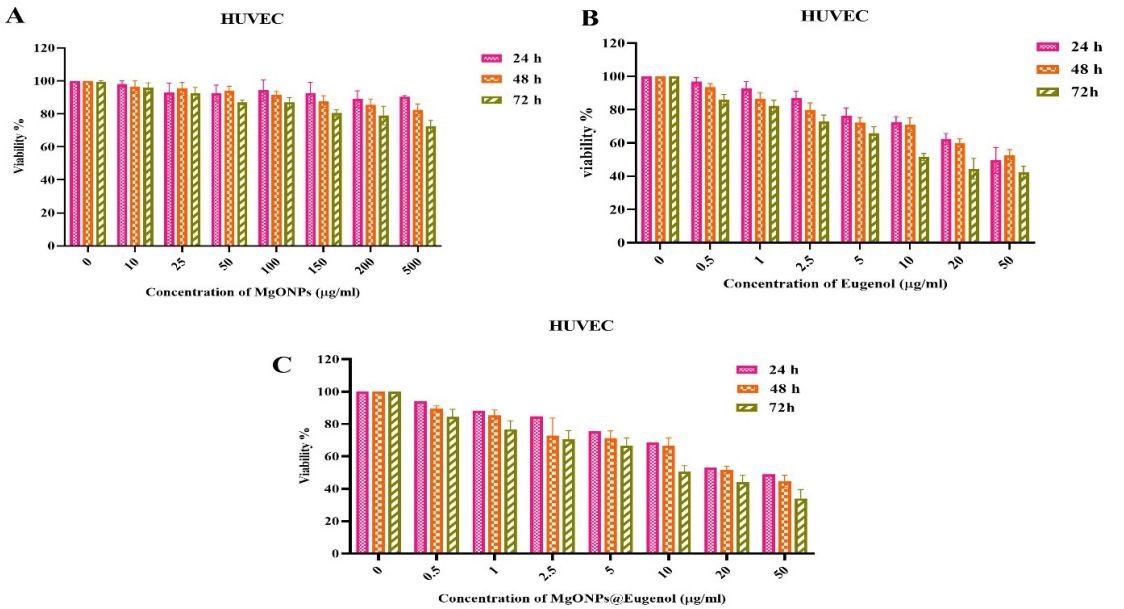

Fig. 4. MTT assay results and cell viability analysis of HUVEC cells after treatment with A) 0-500 µg/mL of bare MgO NPs, B) 0-50 µg/mL of free eugenol, and C) 0-50 µg/mL of MgO NPs @ Eugenol for 24- 72 h.

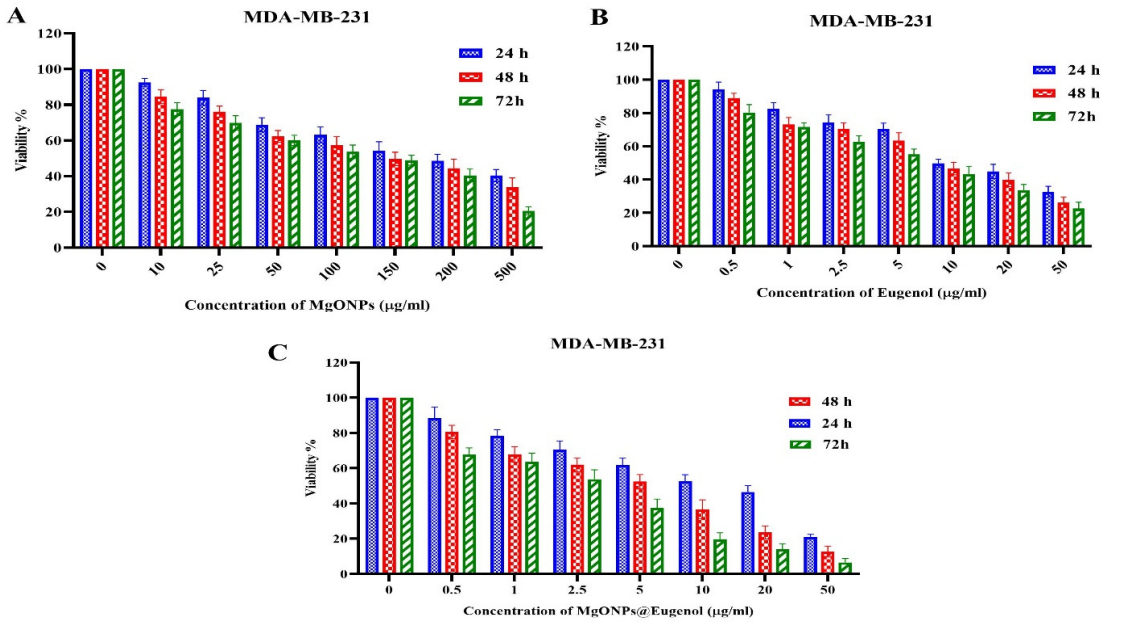

Fig. 5. cell viability analysis of MDA-MB-231 cells after treatment with A) 0-500 µg/mL of bare MgO NPs, B) 0-50 µg/mL of free eugenol, and C) 0-50 µg/mL of MgO NPs@Eugenol for 24- 72 h.

NPs, free eugenol, and MgO NPs@Eugenol were evaluated in MDA-MB-231 breast cancer cells using a wound-healing (scratch) assay. Confluent monolayers of MDA-MB-231 cells were scratched and subsequently treated with the IC_{30} concentrations of each formulation. Sequential microscopic images of the wound area were captured at 0, 24, and 48 h post-treatment, as

Table 2. IC50 value (µg/ml) of bare MgO NPs, free eugenol, and MgO NPs@Eugenol across HUEVC and MDA-MB-231 cells after 24, 48, and 72 h of treatment.

	IC50 (µg/ml) (HUVEC)			IC50 (µg/ml) (MDA-MB-231)		
	24 h	48 h	72 h	24 h	48 h	72 h
MgO NPs	> 1000	> 1000	>1000	245.11±0.29	177.29±0.89	150.04±0.97
Free eugenol	65.49±0.26	72.29±0.57	30.98±0.36	14.19 ± 0.91	9.79 ± 0.402	8.45 ± 0.99
MgO NPs@Eugenol	41.97±0.71	35.84±0.21	15.28±0.37	11.75 ± 0.92	6.18 ± 0.26	3.65 ± 0.51

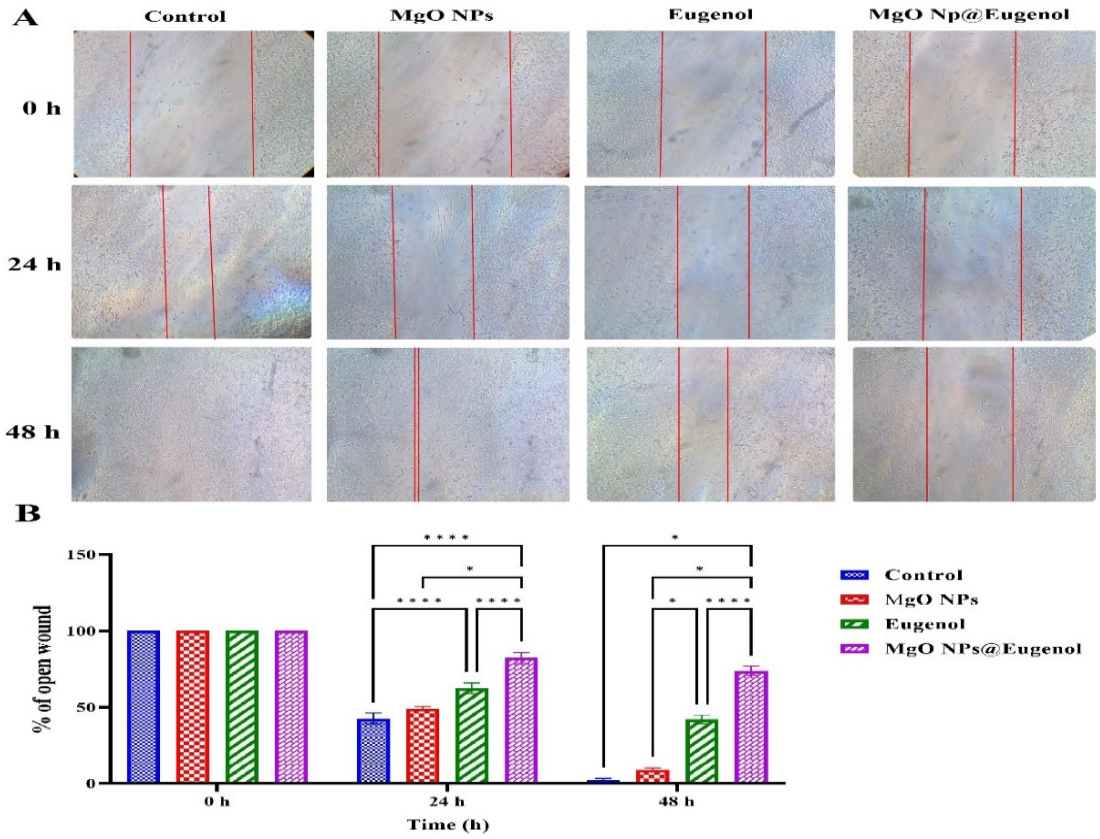

Fig. 6. Scratch assay to investigate the migration of MDA-MB-231 cells after treatment with bare MgO NPs, free eugenol, and MgO NPs@Eugenol. A) Sequential microscopic images and wound closure rates. B) Scratch width ratio calculated using image J through the means of three individuals. * *p*-value less than 0.05.

illustrated in Figure 6A. The percentage of wound closure was quantified using ImageJ software (Figure 6B). At the initial time point (0 h), the wound area was standardized to 100% across all experimental groups. After 24 hours, the control group exhibited a substantial reduction in wound width, reaching approximately 40% closure, consistent with the high intrinsic migratory capacity of MDA-MB-231 cells. In contrast, the wound areas in the treated groups remained significantly wider, indicating impaired cell migration. By 48 h, near-complete wound closure was observed in the control group, whereas cells treated with bare MgO NPs and free eugenol showed moderate inhibition of migration. Notably, the MgO NPs@Eugenol group displayed the most pronounced inhibition, with approximately 75% of the wound area remaining unclosed compared to the control. These findings demonstrate that MgO NPs@Eugenol significantly impairs the migratory ability of MDA-MB-231 cells, suggesting potential anti-metastatic properties of this components.

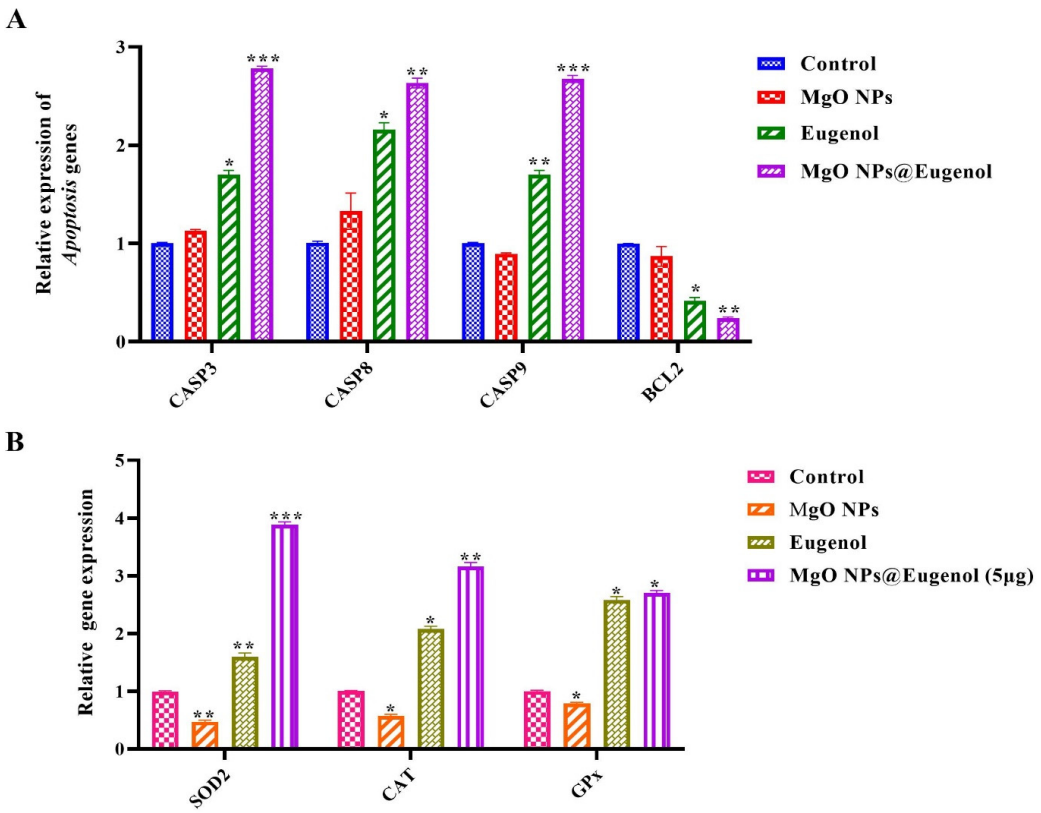

Fig. 7. Gene expression analysis in MDA-MB-231 cells treated with MgO NPs, free eugenol, and MgO NPs @ Eugenol using qPCR. A) Expression levels of apoptosis-associated genes including *CASP3*, *CASP8*, and *CASP9*. (B) Expression of oxidative stress-associated genes, including *SOD2*, *CAT*, and *GPx1*. Gene expression levels were normalized to GAPDH expression levels. *, **, and *** represent p-values of <0.05, 0.005, and 0.0005, respectively.

Gene expression analysis

Gene expression analysis was employed to investigate the effect of treatment with IC50 of bare MgO NPs, free eugenol, and MgO NPs@Eugenol on the expression levels of apoptosis-associated genes such as *CASP3*, *CASP8*, *CASP9*, and *BCL-2*, as well as some oxidative stress-associated genes such as *SOD2*, *CAT*, and *GPx1* in MDA-MB-231 cells. As depicted in Figure 7A, *CASP* genes were significantly upregulated in free eugenol- and MgO NPs@Eugenol-treated cells compared to untreated control cells, whereas *BCL-2* was significantly downregulated in free eugenol- and MgO NPs@Eugenol-treated cells compared to control cells. In addition, the most significant differential expression was observed for *CASP3* and *BCL-2* in free eugenol- and MgO NPs@Eugenol-treated cells compared to the control. No significant changes in the expression levels of apoptosis-associated genes were observed in the bare MgO NP-treated cells compared with those in the control. With respect to oxidative stress-associated genes, Figure 7B demonstrates that treatment with both free eugenol and MgO NPs@Eugenol led to significant upregulation of *SOD2*, *CAT*, and *GPx1* in MDA-MB-231 cells. Notably, the expression levels of these genes were substantially higher in cells treated with MgO NPs@eugenol than in those treated with free eugenol, indicating that the nanoparticle-based delivery system had an enhanced antioxidant response.

DISCUSSION

Breast cancer remains a major global health concern, representing the most commonly diagnosed malignancy and the leading cause of cancer-related mortality among women worldwide. According to recent statistics from the World Health Organization (WHO, 2023), approximately 2.3 million new cases and over 670,000 deaths

were reported globally, underscoring the profound burden of this disease. Despite the availability of multiple therapeutic modalities—including surgery, chemotherapy, radiotherapy, hormonal therapy, and targeted treatments—the prognosis for many patients remains suboptimal. Factors such as therapeutic resistance, off-target drug effects, tumor heterogeneity, and systemic toxicity contribute to reduced treatment efficacy and a high incidence of both acute and chronic adverse effects. These limitations underscore the critical need for the development of more selective, effective, and safer therapeutic strategies that can overcome the inherent challenges of current breast cancer management. (32).

Nanoparticles as an advancement of nanotechnology, possess anticancer, antibacterial, antifungal, antiviral, antioxidant, anti-inflammatory, and anti-infective properties (33-37). In addition, nanoparticle-based drug delivery systems have gained considerable attention in oncology because of their capacity to enhance drug solubility, enable targeted delivery to tumor tissues via the enhanced permeability and retention (EPR) effect, and protect bioactive compounds from degradation. Concurrently, nature-derived compounds have shown promising biological and medical properties, particularly anticancer properties, alone or in combination with chemotherapeutic drugs (38-40); However, their clinical application is hindered by their poor aqueous solubility, volatility, bioavailability, and rapid metabolism. It has been reported that the delivery of these bioactive compounds with nanoparticles can overcome these challenges (41, 42).

MgO NPs have garnered significant attention in the biomedical field because of their diverse applications, including the development of biosensors, cancer diagnostics and treatment, and medical imaging technologies, which are all primarily attributed to their wide range of beneficial characteristics such as notable catalytic activity, high reactivity, superior absorption properties, biocompatibility, non-toxicity, biodegradability, and cost-effectiveness, making them highly suitable for incorporation into various functional and therapeutic materials (43, 44). Studies have also reported MgO NPs as valuable drug delivery systems to enhance the therapeutic potential and efficacy of drugs (45, 46).

Based on the above-mentioned background, the present study focused on the synthesis of MgO NPs and the evaluation of their physicochemical properties, which play a crucial role in determining their biological interactions, biodistribution, safety, and therapeutic potential (47). Therefore, thorough characterization was conducted to ensure a comprehensive understanding of their functional capabilities. The results of our study illustrated that the size, PDI, and zeta potential of synthesized MgO NPs were determined to be 215.2 nm, 0.089, and -15.48mV, respectively, indicating the suitable size, dimension, low dispersity, and surface charge for systemic circulation. Furthermore, FTIR/XRD and SEM/TEM assays indicated the crystalline and spherical structure of the MgO NPs. Then, we explored the potential of MgO NPs as delivery vehicles to enhance the therapeutic efficacy of eugenol which is a bioactive compound of *Syzygium aromaticum* (clove) and is known for its pharmacological properties, against breast cancer cells, thereby addressing both the biological activity and pharmacokinetic limitations of this natural compound. The results demonstrated that the MgO NPs@Eugenol exhibited significantly higher cytotoxicity against MDA-MB-231 breast cancer cell line compared to free eugenol. This enhancement can be attributed to multiple factors, including improved the bioavailability, improved intracellular uptake, controlled release, increased accumulation of the bioactive compound within cancer cells, and synergistic biological mechanisms (17, 48). Furthermore, this nanoparticle formulation appeared to reduce the effective dose required to inhibit cell viability, as the IC50 value of free eugenol and MgO NPs @ Eugenol calculated to be 8.45 ± 0.99 and 3.65 ± 0.51 µg/mL, respectively, after 72 h of treatment in MDA-MB-231 cells, suggesting a potential reduction in systemic toxicity although needs to be validated by *in vivo* experimental design. Moreover, based on scratch assay, the anti-migratory effect of MgO NPs@Eugenol was much stronger than free eugenol in treated-MDA-MB-231 cells as both compared with untreated cells. Then we intended to investigate the effect of free eugenol and MgO NPs@Eugenol on the apoptosis and oxidative stress pathways, through some of their critical hub genes, demonstrating a significant upregulation of *caspase* (*CASP*) genes such as *CASP3, CASP8, and CASP9*, significant downregulation of *Bcl-2* as well as significant upregulation of *SOD2*, *CAT*, and *GPx*. Regarding oxidative stress-associated

genes, treatment with bare MgO NPs led to the downregulation of genes encoding antioxidant enzymes, suggesting a possible impairment in the cellular antioxidant defense mechanism. This decrease in expression may indicate that bare MgO NPs contribute to oxidative stress by reducing the activity of key protective enzymes. In contrast, treatment with free eugenol and a low concentration of MgO NPs@Eugenol resulted in significant upregulation of these antioxidant genes, indicating a potential protective role of eugenol in mitigating oxidative stress by stimulating the production of antioxidant enzymes, either alone or in a controlled nanoparticle formulation. The enhanced anticancer observations of this study align with previous reports demonstrating improved cytotoxic effects of eugenol when delivered via nanocarriers through synergistic mechanisms. For instance, Kurnia P et. al reported that eugenol-loaded chitosan nanoparticles suppressed the migration, inhibit the epithelial-mesenchymal transition (EMT), and induced apoptosis in human HeLa cervical cancer cell line through *CASP3* activation and *Bcl-2* inactivation (49). Li et. al, also determined the efficacy of eugenol-loaded chitosan in inducing apoptosis and inhibiting metastasis in rat C6 glioma cells (50). In addition, Shahbazi et. al also indicated that eugenol-loaded mesoporous silica nanoparticles exerted higher anti-proliferative, anti-migratory, apoptosis inducing, and increasing SOD activity than free eugenol through the upregulation of genes involved in apoptosis such as *CASP3*, *CASP8*, and *CASP9* as well as downregulation of genes involved in metastasis such as *MMP2*, *MMP9*, and *KRAS* (51).

CONCLUSION

To the best of our knowledge, this is the first study to evaluate the anticancer activities of eugenol-loaded magnesium oxide against breast cancer. MgO NPs@Eugenol can more effectively exert antiproliferative and antimigratory activities, and induce expression levels of pro-apoptotic genes and oxidative stress-associated genes compared with free eugenol. Therefore, eugenol loading into MgO NPs can be suggested for the drug delivery fields as a potential therapeutic approach for breast cancer treatment.

CONFLICT OF INTEREST

The authors declare that there are no conflicts of interest.

REFERENCES

1. Xiong X, Zheng LW, Ding Y, Chen YF, Cai YW, Wang LP, et al. Breast cancer: pathogenesis and treatments. Signal Transduct Target Ther. 2025;10(1):49. https://doi.org/10.1038/s41392-024-02108-4
2. Thakur V, Kutty RV. Recent advances in nanotheranostics for triple negative breast cancer treatment. J Exp Clin Cancer Res. 2019;38(1):430. https://doi.org/10.1186/s13046-019-1443-1
3. Ingole S, Vasdev N, Tekade M, Gupta T, Pawar B, Mhatre M, et al. Toxic effects of cancer therapies. In: Public Health and Toxicology Issues Drug Research, Volume 2. Elsevier; 2024. p. 353-79. https://doi.org/10.1016/B978-0-443-15842-1.00004-1
4. Mustapha A, Ismail A, Abdullahi SU, Hassan ON, Ugwunnaji PI, Berinyuy EB. Cancer chemotherapy: a review update of the mechanisms of actions, prospects and associated problems. BIOMED Nat Appl Sci. 2021;1(1):1-19. https://doi.org/10.53858/bnas01010119
5. Torres Quintas S, Canha-Borges A, Oliveira MJ, Sarmento B, Castro F. Nanotherapeutics in Women's Health Emerging Nanotechnologies for Triple-Negative Breast Cancer Treatment. Small. 2024;20(41):2300666. https://doi.org/10.1002/smll.202300666
6. Gholami A, Mousavi SM, Hashemi SA, Ghasemi Y, Chiang WH, Parvin N. Current trends in chemical modifications of magnetic nanoparticles for targeted drug delivery in cancer chemotherapy. Drug Metab Rev. 2020;52(1):205-24. https://doi.org/10.1080/03602532.2020.1734021
7. Pudlarz A, Szemraj J. Nanoparticles as carriers of proteins, peptides and other therapeutic molecules. Open Life Sci. 2018;13(1):285-98. https://doi.org/10.1515/biol-2018-0035
8. Huang C, Zhang Z, Cui W. Marine-derived natural compounds for the treatment of Parkinson's disease. Mar Drugs. 2019;17(4):221. https://doi.org/10.3390/md17040221
9. Andrade S, Nunes D, Dabur M, Ramalho MJ, Pereira MC, Loureiro JA. Therapeutic potential of natural compounds in neurodegenerative diseases: insights from clinical trials. Pharmaceutics. 2023;15(1):212. https://doi.org/10.3390/pharmaceutics15010212
10. Kong YR, Tay KC, Su YX, Wong CK, Tan WN, Khaw KY. Potential of naturally derived alkaloids as multi-targeted therapeutic agents for neurodegenerative diseases. Molecules. 2021;26(3):728. https://doi.org/10.3390/molecules26030728
11. Torres J, Costa I, Peixoto AF, Silva R, Sousa Lobo JM, Silva AC. Intranasal lipid nanoparticles containing bioactive compounds obtained from marine sources to manage neurodegenerative diseases. Pharmaceuticals. 2023;16(2):311. https://doi.org/10.3390/ph16020311
12. Forte M, Conti V, Damato A, Ambrosio M, Puca AA, Sciarretta S, et al. Targeting nitric oxide with natural derived compounds as a therapeutic strategy in vascular diseases. Oxid Med Cell Longev. 2016;2016:7364138. https://doi.org/10.1155/2016/7364138
13. Leuci R, Brunetti L, Poliseno V, Laghezza A, Loiodice F, Tortorella P, et al. Natural compounds for the prevention and treatment of cardiovascular and neurodegenerative diseases. Foods. 2020;10(1):29. https://doi.org/10.3390/foods10010029

14. Shanmugam G. Plant-derived anti-inflammatory agents: a promising alternative for managing chronic inflammation. Nat Prod Res. 2024:1-2. https://doi.org/10.1080/14786419.2024.2386397
15. Sferrazza G, Corti M, Brusotti G, Pierimarchi P, Temporini C, Serafino A, et al. Nature-derived compounds modulating Wnt/β-catenin pathway: a preventive and therapeutic opportunity in neoplastic diseases. Acta Pharm Sin B. 2020;10(10):1814-34. https://doi.org/10.1016/j.apsb.2019.12.019
16. Huang M, Lu JJ, Ding J. Natural products in cancer therapy: Past, present and future. Nat Prod Bioprospect. 2021;11(1):5-13. https://doi.org/10.1007/s13659-020-00293-7
17. Andreani T, Cheng R, Elbadri K, Ferro C, Menezes T, Dos Santos MR, et al. Natural compounds-based nanomedicines for cancer treatment: Future directions and challenges. Drug Deliv Transl Res. 2024;14(10):2845-916. https://doi.org/10.1007/s13346-024-01649-z
18. Rakotondrabe TF, Fan MX, Muema FW, Guo MQ. Modulating inflammation-mediated diseases via natural phenolic compounds loaded in nanocarrier systems. Pharmaceutics. 2023;15(2):699. https://doi.org/10.3390/pharmaceutics15020699
19. Didehdar M, Chegini Z, Shariati A. Eugenol: A novel therapeutic agent for the inhibition of Candida species infection. Front Pharmacol. 2022;13:872127. https://doi.org/10.3389/fphar.2022.872127
20. Elbestawy MK, El-Sherbiny GM, Moghannem SA. Antibacterial, antibiofilm and anti-inflammatory activities of eugenol clove essential oil against resistant Helicobacter pylori. Molecules. 2023;28(6):2448. https://doi.org/10.3390/molecules28062448
21. Damasceno ROS, Pinheiro JLS, Rodrigues LHM, Gomes RC, Duarte ABS, Emídio JJ, et al. Anti-Inflammatory and Antioxidant Activities of Eugenol: An Update. Pharmaceuticals. 2024;17(11):1505. https://doi.org/10.3390/ph17111505
22. Ali M, Ain S, Kumar B, Ain Q. Development and evaluation of eugenol-based gel formulation for analgesic and anti-inflammatory action. Ann Phytomed. 2022;11(1):338-45. https://doi.org/10.54085/ap.2022.11.1.36
23. Kiki MJ. In vitro antiviral potential, antioxidant, and chemical composition of clove (Syzygium aromaticum) essential oil. Molecules. 2023;28(6):2421. https://doi.org/10.3390/molecules28062421
24. Ulanowska M, Olas B. Biological properties and prospects for the application of eugenol-a review. Int J Mol Sci. 2021;22(7):3671. https://doi.org/10.3390/ijms22073671
25. Zari AT, Zari TA, Hakeem KR. Anticancer properties of eugenol: A review. Molecules. 2021;26(23):7407. https://doi.org/10.3390/molecules26237407
26. Khan Y, Sadia H, Ali Shah SZ, Khan MN, Shah AA, Ullah N, et al. Classification, synthetic, and characterization approaches to nanoparticles, and their applications in various fields of nanotechnology: a review. Catalysts. 2022;12(11):1386. https://doi.org/10.3390/catal12111386
27. Danish MSS, Bhattacharya A, Stepanova D, Mikhaylov A, Grilli ML, Khosravy M, et al. A systematic review of metal oxide applications for energy and environmental sustainability. Metals. 2020;10(12):1604. https://doi.org/10.3390/met10121604
28. Mahdavi M, Shahbazi S, Reiisi S, Rigi G. Investigating the cell proliferation and migration inhibition by cerium oxide nanoparticles loaded with doxorubicin in MDA-MB-231 cell line. Nanomed J. 2024;11(4).
29. Chavali MS, Nikolova MP. Metal oxide nanoparticles and their applications in nanotechnology. SN Appl Sci. 2019;1(6):607. https://doi.org/10.1007/s42452-019-0592-3
30. Hornak J. Synthesis, properties, and selected technical applications of magnesium oxide nanoparticles: a review. Int J Mol Sci. 2021;22(23):12752. https://doi.org/10.3390/ijms222312752
31. Abinaya S, Kavitha HP, Prakash M, Muthukrishnaraj A. Green synthesis of magnesium oxide nanoparticles and its applications: A review. Sustain Chem Pharm. 2021;19:100368. https://doi.org/10.1016/j.scp.2020.100368
32. Li Y, Zhang H, Merkher Y, Chen L, Liu N, Leonov S, et al. Recent advances in therapeutic strategies for triple-negative breast cancer. J Hematol Oncol. 2022;15(1):121. https://doi.org/10.1186/s13045-022-01341-0
33. Abo-zeid Y, Williams GR. The potential anti-infective applications of metal oxide nanoparticles: A systematic review. Wiley Interdiscip Rev Nanomed Nanobiotechnol. 2020;12(2):e1592. https://doi.org/10.1002/wnan.1592
34. Irannejad F, Shahbazi S, Reiisi S, Heidari R. Study of the effect of zinc oxide, selenium, and silver nanoparticles on the expression level of oxidative stress-associated genes in ovarian cancer. Med Oncol. 2025;42(2):39. https://doi.org/10.1007/s12032-024-02593-1
35. Pirbalouti MMA, Shahbazi S, Shahraki SS, Reiisi S, Mokhtari A. Study the antifungal effects of green synthesized silver nanoparticles on the Aspergillus niger, Microsporum canis, and Candida albicans. J Microbiota. 2024;1(3). https://doi.org/10.5812/jmb-154535
36. Solaiman MA, Ali MA, Abdel-Moein NM, Mahmoud EA. Synthesis of Ag-NPs developed by green-chemically method and evaluation of antioxidant activities and anti-inflammatory of synthesized nanoparticles against LPS-induced NO in RAW 264.7 macrophages. Biocatal Agric Biotechnol. 2020;29:101832. https://doi.org/10.1016/j.bcab.2020.101832
37. Taghipour F, Shahbazi S, Reiisi S, Shabani L. Novel green synthesis of silver nanoparticles using carotenoid extracted from Kocuria sp.: determination of antioxidant, antimicrobial, and anti-human breast cancer activities. 3 Biotech. 2025;15(4):1-12. https://doi.org/10.1007/s13205-025-04261-1
38. Omidi F, Shahbazi S, Reiisi S, Azhdari S, Karimzadeh MR. Glycyrrhizic acid enhances the anticancer activity of cisplatin in the human ovarian cancer cell line. Toxicol In Vitro. 2023;93:105687. https://doi.org/10.1016/j.tiv.2023.105687
39. Karimzadeh MR, Masoudi Chelegahi A, Shahbazi S, Reiisi S. Co-treatment of silymarin and cisplatin inhibited cell proliferation, induced apoptosis in ovarian cancer. Mol Biol Rep. 2024;51(1):118. https://doi.org/10.1007/s11033-023-09026-8
40. Jalalpour Choupanan M, Shahbazi S, Reiisi S. Naringenin in combination with quercetin/fisetin shows synergistic anti-proliferative and migration reduction effects in breast cancer cell lines. Mol Biol Rep. 2023;50(9):7489-500. https://doi.org/10.1007/s11033-023-08664-2
41. Albuquerque BR, Heleno SA, Oliveira MBP, Barros L, Ferreira IC. Phenolic compounds: Current industrial applications, limitations and future challenges. Food Funct.

2021;12(1):14-29. https://doi.org/10.1039/D0FO02324H
42. Zhuo Y, Zhao Y-G, Zhang Y. Enhancing drug solubility, bioavailability, and targeted therapeutic applications through magnetic nanoparticles. Molecules. 2024;29(20):4854. https://doi.org/10.3390/molecules29204854
43. Saberi A, Baltatu MS, Vizureanu P. Recent advances in magnesium-magnesium oxide nanoparticle composites for Biomedical Applications. Bioengineering. 2024;11(5):508. https://doi.org/10.3390/bioengineering11050508
44. Nejati M, Rostami M, Mirzaei H, Rahimi-Nasrabadi M, Vosoughifar M, Nasab AS, et al. Green methods for the preparation of MgO nanomaterials and their drug delivery, anti-cancer and anti-bacterial potentials: A review. Inorg Chem Commun. 2022;136:109107. https://doi.org/10.1016/j.inoche.2021.109107
45. Sharma MK, Aggarwal N, Kumar R, Panda JJ, Yu C, Ganguli AK. Enhanced drug delivery using surface-roughened MgO@ Silica nanoparticles loaded with doxorubicin. Microporous Mesoporous Mater. 2025;391:113624. https://doi.org/10.1016/j.micromeso.2025.113624
46. Ranathunge TA, Karunaratne D, Rajapakse R, Watkins DL. Doxorubicin loaded magnesium oxide nanoflakes as pH dependent carriers for simultaneous treatment of cancer and hypomagnesemia. Nanomaterials. 2019;9(2):208. https://doi.org/10.3390/nano9020208
47. Raval N, Maheshwari R, Kalyane D, Youngren-Ortiz SR, Chougule MB, Tekade RK. Importance of physicochemical characterization of nanoparticles in pharmaceutical product development. In: Tekade RK, editor. Basic fundamentals of drug delivery. Elsevier; 2019. p. 369-400. https://doi.org/10.1016/B978-0-12-817909-3.00010-8
48. Manzari-Tavakoli A, Babajani A, Tavakoli MM, Safaeinejad F, Jafari A. Integrating natural compounds and nanoparticle-based drug delivery systems: A novel strategy for enhanced efficacy and selectivity in cancer therapy. Cancer Med. 2024;13(5):e7010. https://doi.org/10.1002/cam4.7010
49. Kurnia H, Puruhita D, Nazhif MH, Threevisca RC. Eugenol-loaded chitosan nanoparticle induces apoptosis, inhibits cell migration and epithelial to mesenchymal. Eur J Mol Clin Med. 2020;7(09).
50. Li Z, Veeraraghavan VP, Mohan SK, Bolla SR, Lakshmanan H, Kumaran S, et al. Apoptotic induction and anti-metastatic activity of eugenol encapsulated chitosan nanopolymer on rat glioma C6 cells via alleviating the MMP signaling pathway. J Photochem Photobiol B. 2020;203:111773. https://doi.org/10.1016/j.jphotobiol.2019.111773
51. Shahbazi S, Reiisi S, Heidari R, Raeisi M. Eugenol-loaded mesoporous silica nanoparticles enhance the sensitivity of cisplatin against AGS human gastric adenocarcinoma cell line. J Nanopart Res. 2023;25(4):57. https://doi.org/10.1007/s11051-023-05712-7